Supplementary Information (SI) for Journal of Materials Chemistry C.

Advanced Cobalt-Based Hierarchical and Gradient Armor Catalysts for High-Performance Li-S Batteries over a Wide Temperature Range

Yiding Li,[a] Siqi Wang,[a] Yujun Fu,[a] Ruoan Li,[a] Han Guo[a], Chengtian Lv,[a] Xiaoqiang Yin,[b] Zhibo Yang,[b] Dequan Liu, *[a] and Deyan He *[a]

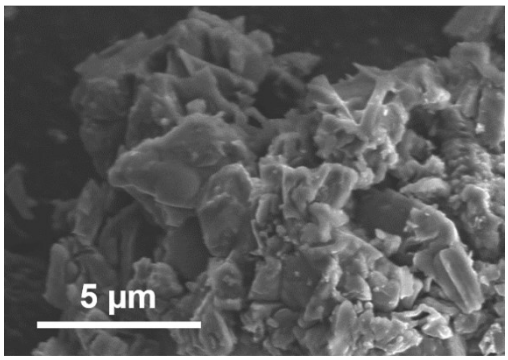

Figure S1. SEM image of the synthesized g-C_3N_4.

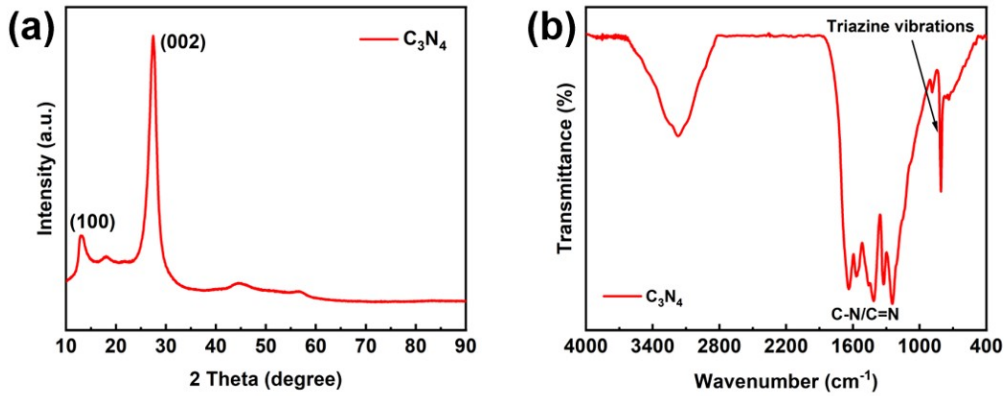

Figure S2. (a) XRD pattern and (b) FTIR spectrum of the synthesized g-C_3N_4.

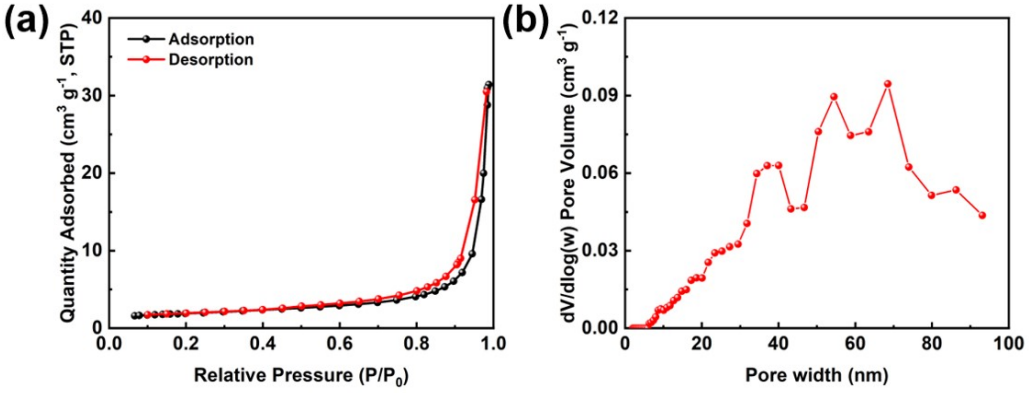

Figure S3. (a) N_2 adsorption-desorption isothermals and (b) pore size distribution of the synthesized g-C_3N_4.

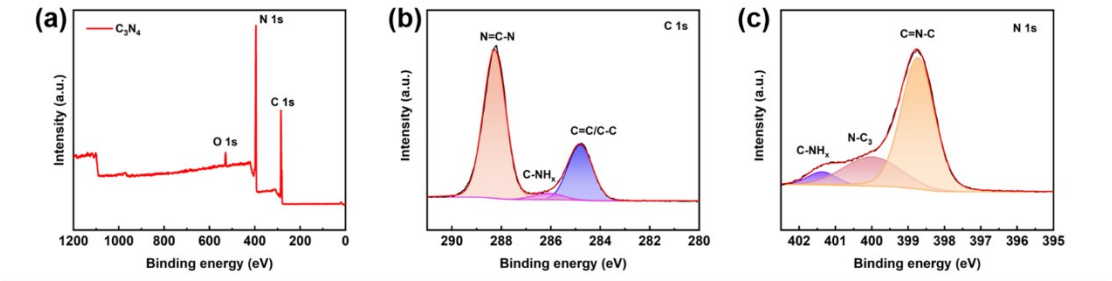

Figure S4. (a) XPS survey scan spectrum, (b) C 1s and (c) N 1s high-resolution XPS spectra of the synthesized g-C_3N_4.

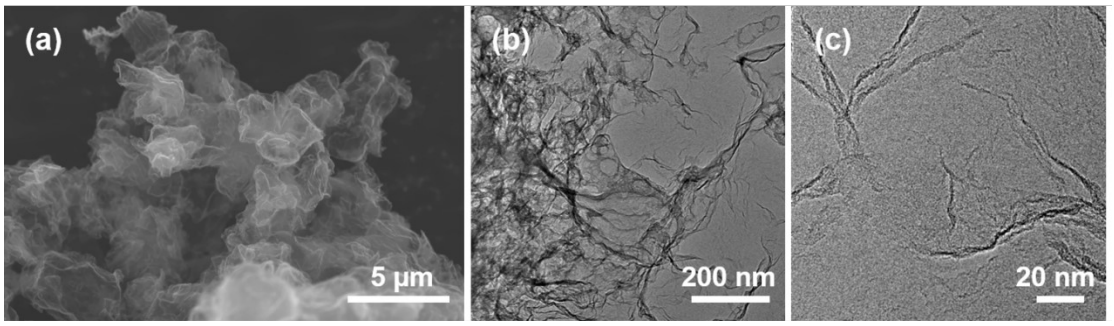

Figure S5. (a) SEM and (b, c) TEM images of the N-doped carbon nanosheets.

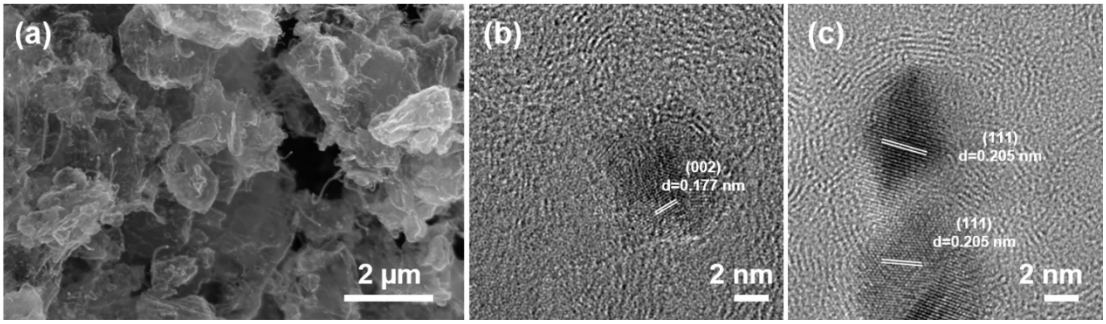

Figure S6. (a) SEM and (b, c) HR-TEM images of Co@NCNN-700.

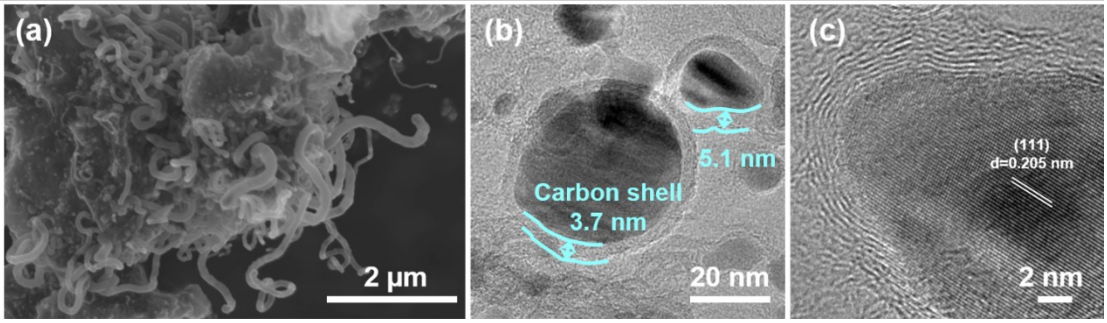

Figure S7. (a) SEM, (b) TEM, and (c) HR-TEM images of Co@NCNN-900.

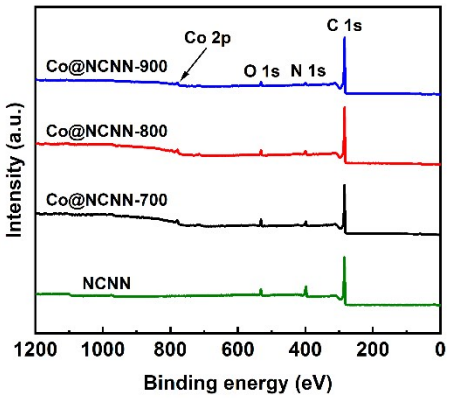

Figure S8. XPS survey scan spectra of the Co@NCNN armor catalysts and NCNN.

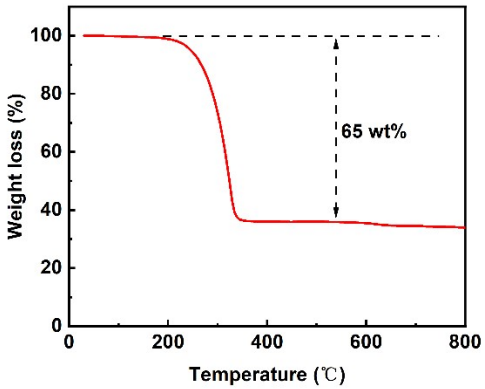

Figure S9. TGA curve of the Co@NCNN-800-S composite in Ar atmosphere.

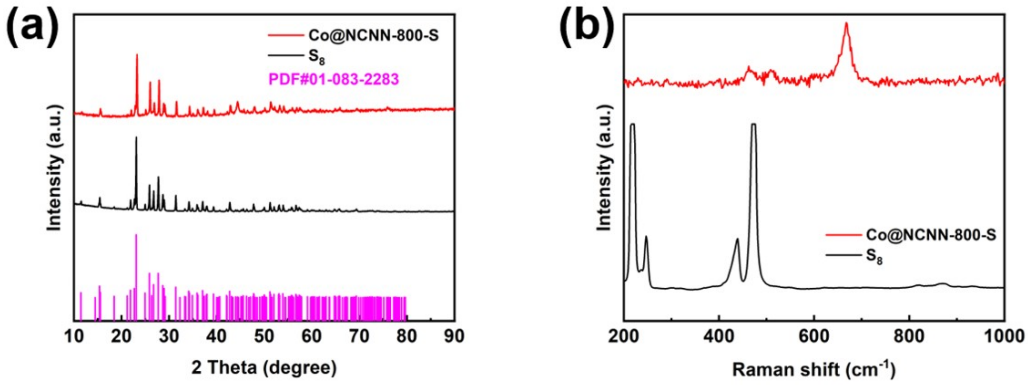

Figure S10. (a) XRD patterns and (b) Raman spectra of Co@NCNN-800-S composite and S_8.

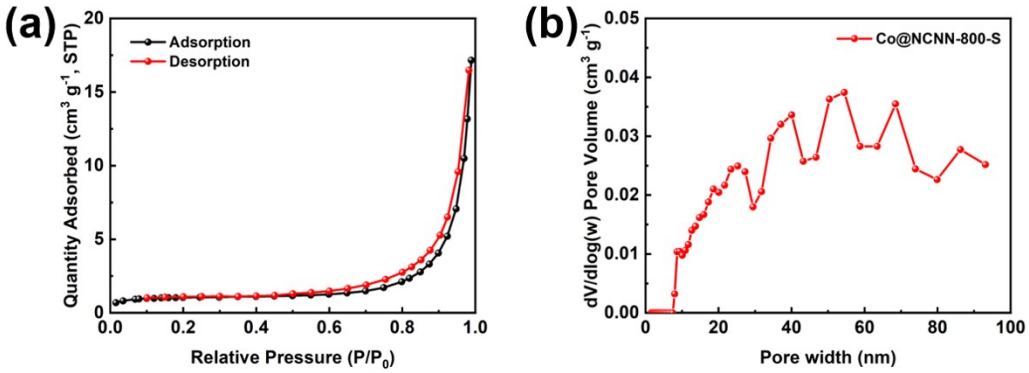

Figure S11. (a) N_2 adsorption-desorption isotherms and (b) pore size distribution of Co@NCNN-800-S composite.

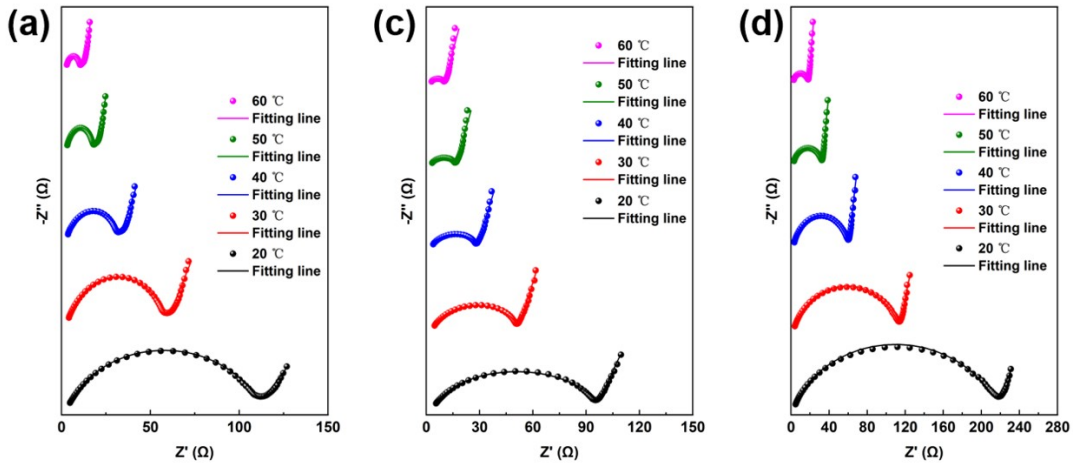

Figure S12. EIS plots of (a) Co@NCNN-700-S, (b) Co@NCNN-900-S, and (c) NCNN-S cathodes at different temperatures and open circuit voltages

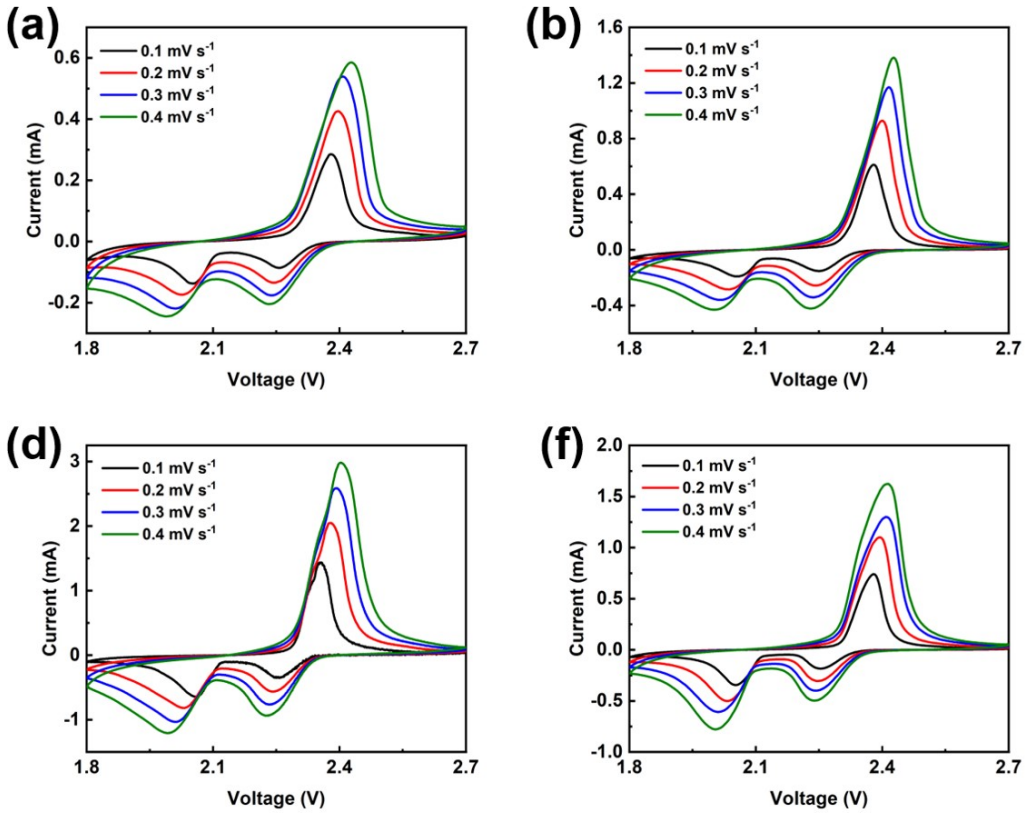

Figure S13. CV curves of Li-S cells with (a) NCNN-S, (b) Co@NCNN-700-S, (c) Co@NCNN-800-S, and (d) Co@NCNN-900-S cathodes at different scan rates from 0.1 to 0.4 mV s^{-1}.

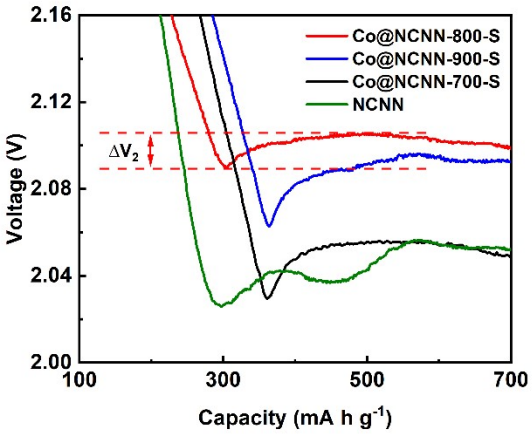

Figure S14. Enlarged view of the charge and discharge profiles in Figure 6c.

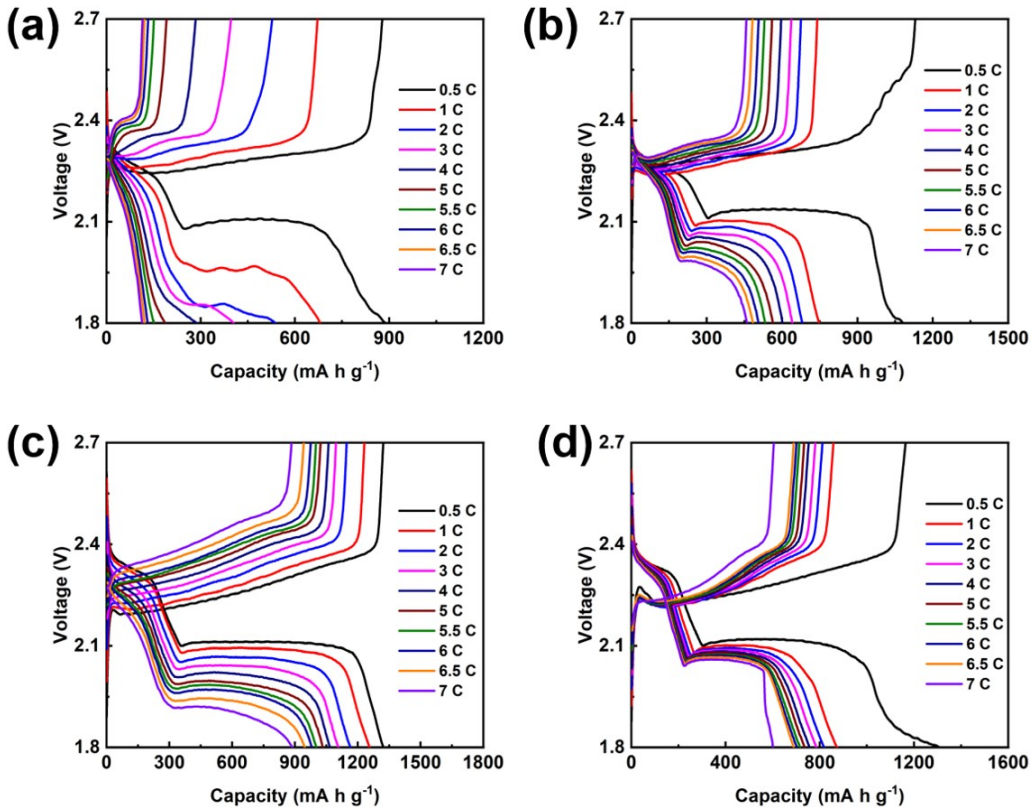

Figure S15. Galvanostatic charge-discharge profiles of Li-S cells with (a) NCNN-S, (b) Co@NCNN-700-S, (c) Co@NCNN-800-S, and (d) Co@NCNN-900-S cathodes at different current densities.

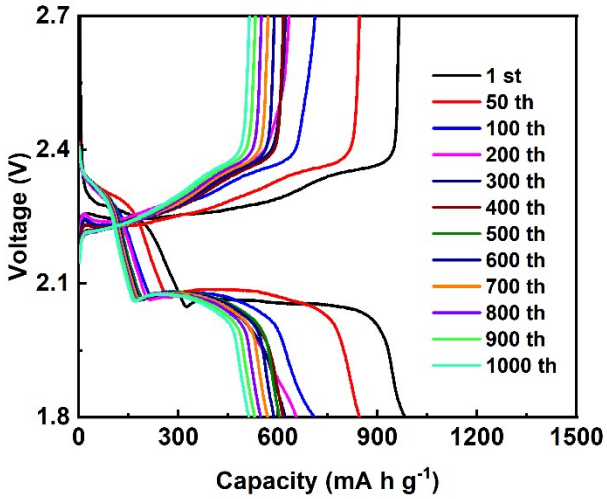

Figure S16. Galvanostatic charge-discharge profiles of Li-S cells with Co@NCNN-800-S electrodes at different cycles under 7 C.

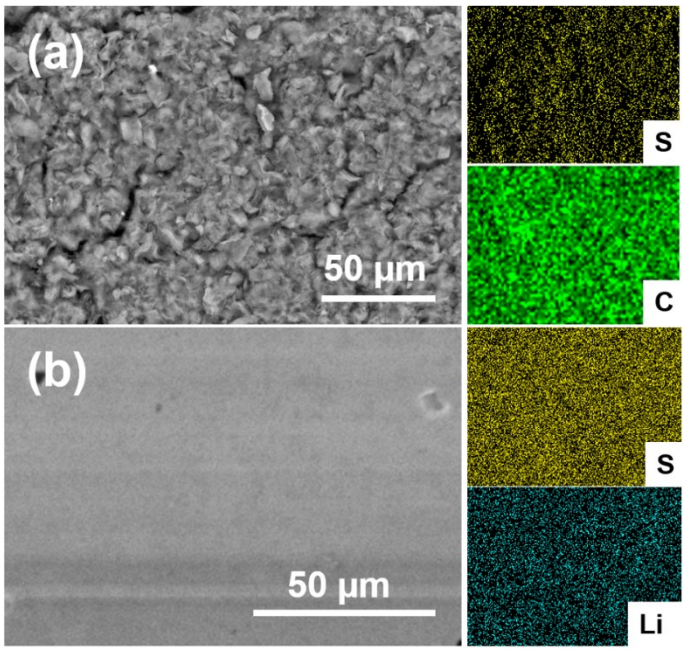

Figure S17. SEM and corresponding element distribution of (a) cathode and (b) lithium anode after cycling.

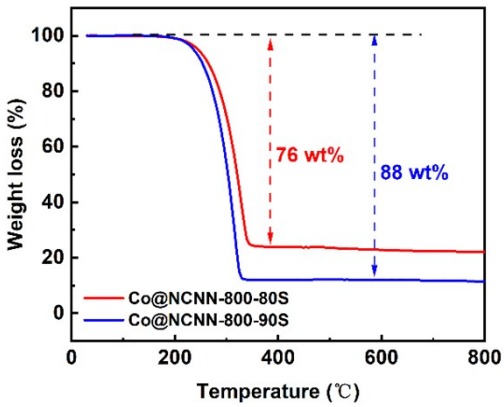

Figure S18. TGA curves of Co@NCNN-800-80S and Co@NCNN-800-90S composites under Ar atmosphere.

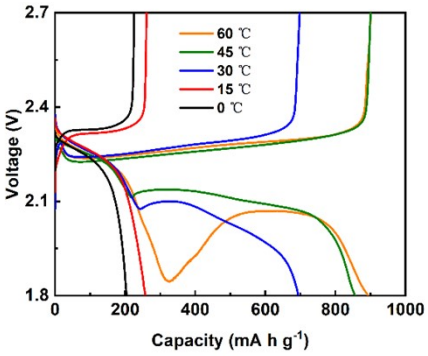

Figure S19. Galvanostatic charge-discharge profiles of the Li-S cell with the NCNN-800-S cathode

at different temperatures.

Table S1. N_2 adsorption-desorption analyses of different samples.

Samples	BET surface area (m^2 g^{-1})	Pore volume (cm^3 g^{-1})
Co@NCNN-900	348.56	1.094
Co@NCNN-800	362.65	0.809
Co@NCNN-700	140.57	0.419
NCNN	113.74	0.297
g-C_3N_4	6.49	0.0048
Co@NCNN-800-S	3.25	0.026

Table S2. Element content in the samples derived from fitting XPS peaks.

Samples	N	O
Co@NCNN-900	3.46%	2.82%
Co@NCNN-800	4.60%	3.24%
Co@NCNN-700	6.67%	4.91%
NCNN	12.28%	4.02%

Table S3. Functional group contents of different samples derived from fitting the XPS peak of C 1s.

	C-C	C-N	C=O
Co@NCNN-900	55.5%	36.2%	8.3%
Co@NCNN-800	53.8%	36.8%	9.4%
Co@NCNN-700	52.9%	35.1%	12.0%
NCNN	57.6%	33.4%	9.0%

Table S4. Functional group contents of different samples derived from fitting the XPS peak of N 1s.

Samples	Graphitic N	Pyridinic N
Co@NCNN-900	61.9%	38.1%
Co@NCNN-800	53.1%	46.9%
Co@NCNN-700	47.1%	52.9%
NCNN	48.9%	51.1%

Table S5. Electrochemical impedance of Li-S batteries with different cathodes at different temperatures and open circuit voltages.

	Co@NCNN-700-S		Co@NCNN-800-S		Co@NCNN-900-S		NCNN-S	
	R_s (Ω)	R_{ct} (Ω)	R_s (Ω)	R_{ct} (Ω)	R_s (Ω)	R_{ct} (Ω)	R_s (Ω)	R_{ct} (Ω)
20 ℃	4.77	107.31	5.11	56.30	5.54	91.30	4.80	211.41
30 ℃	4.16	56.08	4.20	29.78	4.68	47.59	4.14	110.32
40 ℃	3.67	29.80	3.53	15.92	3.94	25.08	3.63	57.42
50 ℃	3.31	16.27	3.11	8.74	3.36	13.66	3.25	30.00
60 ℃	3.02	8.88	2.79	4.91	2.99	7.62	2.95	15.72

Table S6. D_{Li^+} of various samples derived from the Randles-Sevcik equation.

Samples	D_{Li^+} (Peak A)	D_{Li^+} (Peak B)	D_{Li^+} (Peak C)
NCNN	1.97×10^{-10}	1.68×10^{-10}	1.29×10^{-9}
Co@NCNN-700-S	9.71×10^{-10}	7.82×10^{-10}	8.08×10^{-9}
Co@NCNN-800-S	4.64×10^{-9}	4.46×10^{-9}	3.30×10^{-8}
Co@NCNN-900-S	1.29×10^{-9}	2.36×10^{-9}	9.82×10^{-9}

Table S7. Comparison of the performance of Co@NCNN with other Co-based catalysts reported in the literature.

Samples	Sulfur loading (mg cm^{-2})	Highest capacity (mA h g^{-1})	Highest areal capacity (mA h cm^{-2})	Current density	Capacity decay per cycle & Cycles	Reference
Co@NCNN	1.5	1417.7		0.5 C	0.11%, 100 cycles	This work
		983.9		7 C	0.048%, 1000 cycles	
	3.6		3.43	1 C		
	6.1		5.05			
Co-NCNT	2.7	872.3		1 C	0.072%, 700	10.1039/c9cc08218b
	4.3		5.09	0.1 C		
CoP/C	1.4	938		1 C	0.08%, 500	10.1021/acsami.9b18723
	3.2		2.42	0.5 C		
Co-N-C/rGO/PP	1-1.2	865		0.5 C	0.057%, 500	10.1016/j.memsci.2017.11.026
Co/Ti_2C	1.1	880		0.2 C	0.087%, 400	10.1002/smll.202204005
CoOOH-PHCS	5.0	1040		0.1 C	0.485%, 100	10.1016/j.cej.2022.135790
rGO/a-CoO NSs	2.0	1248.2		1 c	0.033%, 500	10.1038/s41467-021-23349-9
Co_9S_8/CoO	1	956		1 C	0.065 %, 300 cycles	10.1016/j.nanoen.2019.03.060
	2.5	925		1 C	0.049%, 1000 cycles	
Co-NiS_2@CNF-CNT	1.8	1218		0.2	0.045%, 500 cycles	10.1002/aenm.202300452
S-Z-CoS_2		993		0.2 C	0.12%, 200 cycles	10.1039/c9ta06947j
	2.5-2.9		3	0.2 C		

Note 1. The content of Co in the Co@NCNN armor catalyst.

At 800 ℃ in an air environment, the catalyst undergoes oxidation, resulting in carbon loss and the eventual oxidation of cobalt to Co_3O_4 ($3Co+2O_2 \rightarrow Co_3O_4$). The content of Co in the sample can be accurately determined through calculations based on the reaction equation.

Assume that the 1 g sample before heating contains x g ($\frac{x}{59} mol$) of Co. The amount of substance reacting the final Co_3O_4 is $\frac{1}{3} \times \frac{x}{59} mol$. According to the TGA curve (Figure 2b), the residual mass of the Co@NCNN-700, Co@NCNN-800, and Co@NCNN-900 are 0.4108, 0.3923 and 0.3583 g, respectively. The Co content before the reaction can be obtained by the following equation:

$$\frac{1}{3} \times \frac{x}{59} \times (59 \times 3 + 16 \times 4) = 0.4108 \text{ or } 0.3923 \text{ or } 0.3583$$

According to the calculation, the Co content of Co@NCNN-700, Co@NCNN-800, and Co@NCNN-900 are 30.2, 28.8 and 26.3 wt%, respectively.

Note 2. Calculation of lithium-ion diffusion coefficient (D_{Li^+})

Lithium-ion diffusion coefficient (D_{Li^+}) can be calculated according to the Randles-Sevcik equation:

$$I_p = 2.65 \times 10^5 n^{1.5} A D_{Li^+}^{0.5} C_{Li^+} v^{0.5}$$

In the equation, I_p is the peak current (A), n is the number of transferred electrons (n = 2 in Li-S battery), A is the electrode area (A=1.33 cm^{-2}), D_{Li^+} is the diffusion rate of Li^+ ($cm^2\ s^{-1}$), C_{Li^+} is the concentration of Li^+ in electrolyte (C_{Li^+} = 1 mol L^{-1}), and v is the scan rate.

The above equation can be obtained by deformation:

$$D_{Li^+} = \left(\frac{1}{2.65 \times 10^5 \times 2^{1.5} \times 1.33} \times \frac{I_p}{v^{0.5}}\right)^2$$

Thus, the D_{Li^+} can be calculated from the linear relationship between the peak current and the square root of the scan rate.